Terahertz Field Enhancement and Photon-Assisted Tunneling in Single-Molecule Transistors

Kenji Yoshida,[1,*] Kenji Shibata,[1,2,†] and Kazuhiko Hirakawa[1,2,‡]
[1]Center for Photonics Electronics Convergence, Institute of Industrial Science, University of Tokyo, 4-6-1 Komaba, Meguro-ku, Tokyo 153-8505, Japan
[2]Institute for Nano Quantum Information Electronics, University of Tokyo, 4-6-1 Komaba, Meguro-ku, Tokyo 153-8505, Japan
(Received 6 March 2015; revised manuscript received 31 August 2015; published 23 September 2015)

We have investigated the electron transport in single-C_{60}-molecule transistors under the illumination of intense monochromatic terahertz (THz) radiation. By employing an antenna structure with a sub-nm-wide gap, we concentrate THz radiation beyond the diffraction limit and focus it onto a single molecule. Photon-assisted tunneling (PAT) in the single molecule transistors is observed in both the weak-coupling and Kondo regimes. The THz power dependence of the PAT conductance indicates that when the incident THz intensity is a few tens of mW, the THz field induced at the molecule exceeds 100 kV/cm, which is enhanced by a factor of $\sim 10^5$ from the field in the free space.

DOI: 10.1103/PhysRevLett.115.138302 PACS numbers: 82.37.-j, 73.23.Hk, 78.40.Ri, 85.35.-p

Tunneling in the presence of time-varying fields has been attracting considerable interest, and interesting phenomena have been observed such as a single-electron pump [1], a single-electron turnstile [1], and photon-assisted tunneling (PAT) [2–6]. Transport in single-electron transistors (SETs) under ac fields shows various behaviors that depend on the relationship between the ac frequency and the tunneling time of electrons. In particular, in the high-ac-frequency regime where the condition $hf \gg \Gamma$ is satisfied (h, f, and Γ are the Planck constant, the frequency of the ac field, and the tunneling rate, respectively), tunneling electrons in the SET are subjected to a time-varying potential and the ac fields must be treated quantum mechanically. In this regime, electron-photon interactions become observable and intriguing quantum mechanical phenomena such as PAT are expected.

Recently, electron transport through single molecules has been attracting considerable attention owing to its potential to realize a variety of molecular functions for electronics [7–11]. So far, most of the works on single-molecule transport have been performed on their static properties and very little has been done on dynamical transport. Typical energy scales in single-molecule transport (e.g., tunneling times, vibron energies, orbital energy spacings, charging energies, etc.) lie mostly in the terahertz (THz) frequency range. To study the interactions between strong THz fields and single molecules, however, we must greatly exceed the diffraction limit and focus long-wavelength THz radiation onto a single molecule. Recent studies have shown that the plasmonic effects of metal electrodes with a nanometer-scale gap can efficiently focus electromagnetic fields into the gap region [12–16]. The use of such nanogap structures may allow us to investigate how electron-photon interactions affect the charge transport through single molecules.

Here, we report on the electron transport in single C_{60}-molecule transistors under the illumination of monochromatic THz radiation at 2.5 THz with an intensity of a few tens of mW. Using the electrical break junction (EBJ) method, we have fabricated a sample structure that can focus THz radiation onto a single molecule trapped between nanogap electrodes. When the samples are illuminated with THz radiation, they exhibit satellite conductance lines that arise from PAT. From the power dependence of the PAT conductance, we have found that the THz electric field induced across the nanogap electrodes exceeds 100 kV/cm, which is enhanced from its value in the free space by a factor of $\sim 10^5$. Furthermore, we have investigated the interaction between intense THz fields and single-molecule transistors (SMTs) in the strong tunnel coupling regime and observed the photon-induced Kondo satellites.

We fabricated SMTs by the EBJ method [17,18]. Figure 1(a) shows a schematic illustration of the sample structure used in this work. An 8-nm-thick NiCr layer, which served as a semitransparent backgate electrode, was deposited on a semi-insulating GaAs substrate, and a 30-nm-thick Al_2O_3 gate-insulation film was grown by atomic layer deposition. We formed thin gold nanojunctions for the source and drain electrodes on the surface of the wafer by the shadow evaporation technique. To achieve a good coupling efficiency between the THz radiation and the tunneling electrons, we employed a bowtie-shaped antenna for the source and drain electrodes, as shown in Fig. 1(b). Since the fabrication yield of SMTs is low (typically a few %), we fabricated 11 nanojunctions on a chip by inserting slits into the bowtie-shaped drain electrode. The chip was then glued with polymethylmethacrylate (PMMA) on a hemispherical silicon lens to tightly focus the THz radiation on the bowtie antenna. A dilute

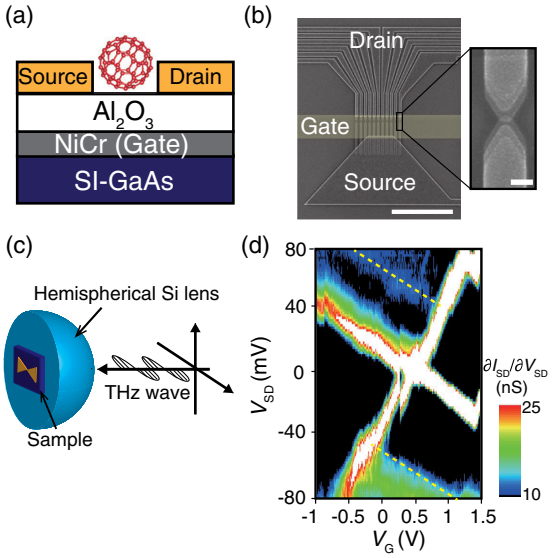

FIG. 1 (color online). (a) Schematic illustration of the sample structure. (b) Scanning electron microscopy (SEM) image of the fabricated sample with a bowtie antenna structure. The scale bar corresponds to 10 μm. The inset shows an SEM image of a metal nanocontact. The scale bar corresponds to 200 nm. (c) Schematic illustration of the fabricated sample mounted on a hemispherical silicon lens. (d) Coulomb stability diagram of a single C_{60}-molecule transistor. The yellow dashed lines indicate the excited states that correspond to the excitation of the internal vibrational mode ($H_g(1)$ mode) of the C_{60} molecule.

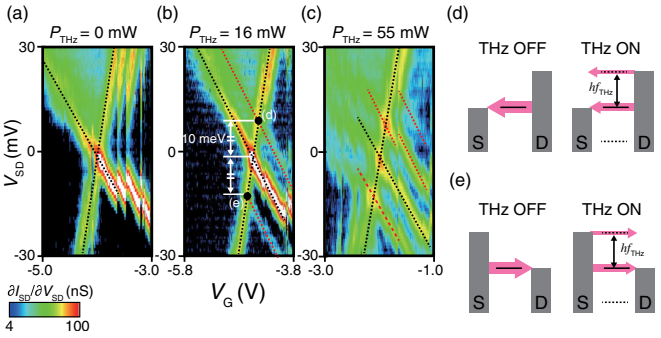

FIG. 2 (color online). (a)–(c) Coulomb stability diagrams measured under the illumination of 2.5 THz radiation for P_{THz} = 0 (a), 16 (b), and 55 mW (c). The black dotted lines represent the boundaries between the transport and Coulomb blockaded regions. The red dotted lines show the differential conductance peaks generated by the THz radiation. (d), (e) Energy band diagrams when the photon-assisted tunneling process occurs at the bias points indicated by the black dots in (b). The dotted lines denote photon sidebands created by the THz radiation.

toluene solution of C_{60} molecules was deposited onto the surface of the gold nanojunctions and dried with nitrogen gas. The sample chip was then mounted into a ^{4}He cryostat. We applied the feedback-controlled EBJ process to the metal nanojunctions to create atomic-scale gaps. Details of the feedback control of the EBJ process have been described elsewhere [19–21]. The THz radiation used in this work was generated by pumping methanol gas with a CO_2 laser. The frequency of the radiation was 2.5 THz (wavelength $\lambda = 119$ μm; photon energy $hf = 10.3$ meV). The radiation was incident from the backside of the samples through the silicon lens with the polarization parallel to the axis of the bowtie antenna [see Fig. 1(c)]. Figure 1(d) shows a color-coded differential conductance ($\partial I_{SD}/\partial V_{SD}$) map of a SMT sample as a function of V_{SD} and V_G. As seen in the figure, the excitation of an internal molecular vibration mode at ~35 meV [7], which is intrinsic to the C_{60} molecule, can be observed in the Coulomb stability diagram, confirming that a single C_{60} molecule is trapped between the nanogap in the electrodes and serves as a Coulomb island. The tunneling conductance of the sample was approximately $4 \times 10^{-5} e^2/h$, where e is the elementary charge, and this sample operated in the weak coupling regime.

Figures 2(a)–2(c) show Coulomb stability diagrams of the sample in Fig. 1(d) measured under three different incident THz radiations with intensities of $P_{THz} = 0$, 16, and 55 mW, respectively. P_{THz} was measured at the exit of the laser. The jagged feature that appears in the range of -3.6 V $< V_G < -3.2$ V in Fig. 2(a) is due to charge trapping or detrapping at nearby defects and is not important. As seen in Fig. 2(b), additional $\partial I_{SD}/\partial V_{SD}$ lines parallel to the ground-state lines (i.e., the boundaries of the Coulomb diamonds) appear in both the single-electron transport and Coulomb blockaded regions, which suggests that additional electron tunneling pathways are created by the THz radiation. From the stability diagram shown in Fig. 2(b), the energy separations between the ground-state line and the satellite lines are determined to be ± 10 meV, which agrees with the photon energy of the THz radiation ($hf = 10.3$ meV). The emergence of the satellite lines indicates that photon sidebands are formed in the system by the THz irradiation and that the tunneling through the photon sidebands, i.e., PAT, becomes possible, as schematically shown in Figs. 2(d) and 2(e). The observation of PAT in the SMTs is remarkable, since it means that the focusing of long-wavelength THz radiation on a single molecule has been achieved by using the metal nanogap electrodes, where the THz radiation is beyond the diffraction limit by a factor of $\sim 10^5$. When P_{THz} is increased to 55 mW, not only do the satellite peaks at ± 10 meV grow in magnitude but also a new satellite peak appears at 20 meV above the ground-state line, indicating that two-photon absorption takes place when P_{THz} is increased. In contrast, the tunnel conductance for the ground state line is reduced with increasing P_{THz}.

The conductance for N-photon PAT, G_N, is known to be proportional to $J_N{}^2(\alpha)$, where J_N is the Nth-order Bessel function and $\alpha = eV_{THz}/hf$ [2]. V_{THz} is the THz voltage induced across the nanogap. The ratio of the conductance of the Nth satellite G_N to the ground-state conductance G_0 is then given by $G_N/G_0 = J_N{}^2(\alpha)/J_0{}^2(\alpha)$. Figure 3 plots

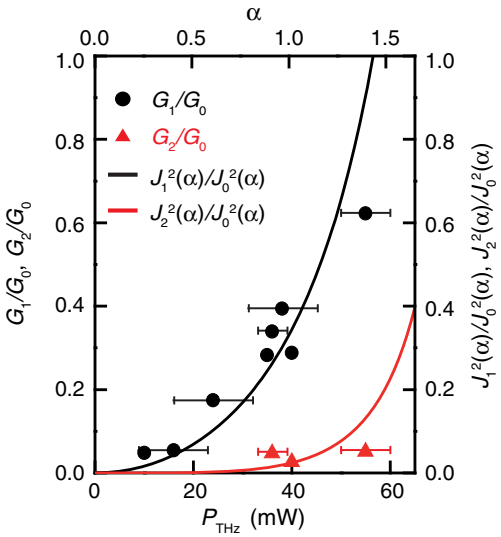

FIG. 3 (color online). P_{THz} dependence of G_1/G_0 (black dots) and G_2/G_0 (red dots). The black and red curves indicate ${J_1}^2(\alpha)/{J_0}^2(\alpha)$ and ${J_2}^2(\alpha)/{J_0}^2(\alpha)$ as a function of α, respectively.

the conductance ratios G_1/G_0 and G_2/G_0 as a function of P_{THz}. The black curve is drawn by fitting ${J_1}^2(\alpha)/{J_0}^2(\alpha)$ to the $N = 1$ data. As seen in Fig. 3, the experimental data for G_1/G_0 are well fitted by ${J_1}^2(\alpha)/{J_0}^2(\alpha)$, which supports that the satellite channels are indeed created by the PAT effect. The red curve for $N = 2$ is drawn by using the same α determined by fitting for the $N = 1$ data. The reasonable agreement for $N = 2$ confirms the consistency of the obtained α. Note that α is on the order of unity when $P_{\mathrm{THz}} \geq 36$ mW. Since the nanogap distance d is comparable to the size of a C_{60} molecule (diameter ~0.7 nm), $\alpha \equiv eV_{\mathrm{THz}}/hf \sim 1$ indicates the remarkable fact that the THz field in the gap, E_{THz}, exceeds 100 kV/cm ($E_{\mathrm{THz}} = V_{\mathrm{THz}}/d \sim hf/ed > 100$ kV/cm). Since E_{THz} in the free space is of the order of V/cm under the experimental conditions in this work, this means that the THz field at the molecule is enhanced by a factor of $\sim 10^5$ from its free-space value by the plasmonic effect of the metal nanogap electrodes. This large field enhancement is of the order of λ/d (λ is the THz wavelength and d the nm-scale gap width).

When the tunnel coupling between a quantum dot and its surrounding leads is strong and the quantum dot contains an unpaired electron, the unpaired electron antiferromagnetically couples with the electrons in the leads, resulting in the formation of the Kondo resonance at the Fermi level E_F of the leads. In this situation, a spin-flip elastic cotunneling process through the Kondo resonance starts participating in the charge transport. Although the dc Kondo effect in a quantum dot has been extensively studied, it will be very interesting to investigate how the Kondo many-body state is affected by external ac fields. So far, only a few experimental works on the dynamics of the Kondo effect have been reported [22–26], although it has been discussed theoretically [27–29]. Recent transport experiments on SMTs have demonstrated clear signatures of the Kondo effect [8,30]. In particular, extremely high Kondo temperatures T_K ranging from 30 to 150 K have been observed in C_{60}-based SMTs [30–32] and $k_B T_K$ lies in the THz frequency range (k_B is the Boltzmann constant). Therefore, the ac frequency must be in the THz range to modulate the Kondo states with such a high T_K.

Figure 4(a) shows the Coulomb stability diagram of a C_{60} SMT that has a tunnel conductance of $2 \times 10^{-3} e^2/h$ and operates in the strong coupling regime measured at 5 K. In this sample, the C_{60} molecule had a weak gate coupling and we were not able to access a charge degeneracy point; the stability diagram shown in Fig. 4(a) corresponds to a part of the Coulomb blockaded region. As seen in the figure, a high differential conductance line appears along $V_{\mathrm{SD}} = 0$. We measured the $\partial I_{\mathrm{SD}}/\partial V_{\mathrm{SD}}$ spectra at $V_G = 0$ V and found a resonant conductance peak at $V_{\mathrm{SD}} = 0$ mV [see Fig. 4(b)]. Figure 4(c) plots the height of the zero-bias conductance peak as a function of T. The peak height is well fitted by the following semiempirical form for the differential conductance of the spin-1/2 Kondo resonance:

$$\partial I_{\mathrm{SD}}/\partial V_{\mathrm{SD}}(T) = G_C[1 + (2^{1/s} - 1)(T/T_K)^2]^{-s}, \quad (1)$$

where G_C is a constant [33]. We used the value of $\partial I_{\mathrm{SD}}/\partial V_{\mathrm{SD}}$ measured at $T = 5$ K for $G_C (= 2.48 \times 10^{-3} e^2/h)$ and set s to 0.22. From this fitting, we confirmed that the conductance peak at $V_{\mathrm{SD}} = 0$ is indeed the Kondo resonance and determined T_K to be ~65 K, which is consistent with T_K observed in the previous work on C_{60} SMTs [30–34]. This value agrees with T_K estimated from the full width at half maximum of the resonant conductance peak in Fig. 4(b)[13,30].

Figure 4(d) shows the $\partial I_{\mathrm{SD}}/\partial V_{\mathrm{SD}}$ spectra of the sample measured under 2.5 THz radiation for three different P_{THz} values (=0, 30, and 56 mW). As shown in the figure, the zero-bias conductance peak decreases in magnitude with increasing P_{THz} and new satellite shoulders appear at $V_{\mathrm{SD}} \sim \pm 10$ mV, which correspond to the THz photon energy ($hf_{\mathrm{THz}} = 10.3$ meV). Furthermore, the satellite shoulders grow with increasing P_{THz}. Note that no broadening of the Kondo peak is discernible under the THz irradiation, indicating that the suppression of the zero-photon Kondo peak is not due to heating by the THz illumination. The Kondo satellite peak on the positive-bias side is less apparent than that on the negative-bias side. This is probably due to asymmetry in the tunnel couplings of the C_{60} molecule to the source and drain electrodes in the present sample [35]. Figure 4(e) shows an example of peak-fitting analysis for the $\partial I_{\mathrm{SD}}/\partial V_{\mathrm{SD}}$ spectrum measured at $P_{\mathrm{THz}} = 56$ mW [36]. The Kondo satellite peaks can be seen for both polarities. As done in the weak

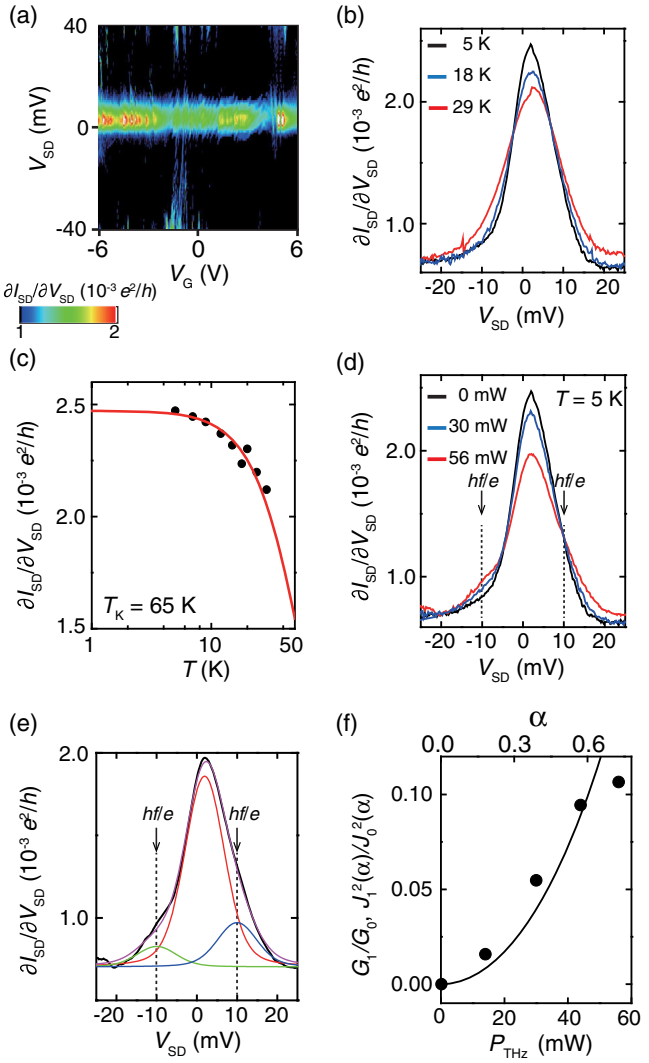

FIG. 4 (color online). (a) Coulomb stability diagram of a C_{60} SMT in the strong coupling regime. (b) Differential conductance spectra measured at 5, 18, and 29 K (top to bottom). (c) Temperature dependence of the Kondo resonant peak height. The red solid line is a fit to the experimental data using the semiempirical functional form for the spin-1/2 quantum dot with $T_K = 65$ K. (d) Differential conductance spectra measured at 5 K under the illumination of 2.5 THz radiation for $P_{THz} = 0$, 30, and 56 mW (top to bottom). (e) Differential conductance spectrum measured at 5 K under the illumination of 2.5 THz radiation at $P_{THz} = 56$ mW (black). The red, green, and blue curves are the fitting curves for the main Kondo peak, the satellite Kondo peaks on the negative- and positive-bias sides, respectively. The violet curve is the resulting sum of the three fitting curves. (f) P_{THz} dependence of G_1/G_0. $J_1^2(\alpha)/J_0^2(\alpha)$ is plotted as a function of α by a black curve.

coupling regime, we plot G_1/G_0 as a function of P_{THz} in Fig. 4(f), where G_0 and G_1 are the conductances of the main peak and satellite peak on the negative-bias side, respectively. We used G_1 only for the negative bias, because the fitting for G_1 on the positive-bias side is more ambiguous and may induce large errors. In the figure, $J_1^2(\alpha)/J_0^2(\alpha)$ is also plotted as a function of α. G_1/G_0 is well fitted by the $J_1^2(\alpha)/J_0^2(\alpha)$ dependence, indicating that the satellite conductance peak arises from the PAT process.

To modulate the Kondo state by photons, two conditions must be satisfied simultaneously: (i) $hf > k_B T_K$ and (ii) $eV_{THz} \sim hf$ [22]. It is predicted that when an electromagnetic wave at frequency f is incident on a SET in the Kondo regime and these two conditions are satisfied, photon-induced satellite peaks are formed in the Kondo resonance at $E_F \pm nhf$, where n is an integer, resulting in the differential conductance peaks at $V_{SD} = \pm nhf/e$. Since T_K for the present sample is 65 K and the THz frequency f is 2.5 THz, the first condition $hf > k_B T_K$ is satisfied. Furthermore, V_{THz} is estimated to be 2–6 mV from the fitting shown in Fig. 4(f) and is of the same order as hf/e. This means that the second condition is also satisfied. As seen in Fig. 4(d), the satellite peak height increases with increasing P_{THz}, while the zero-photon Kondo peak at $V_{SD} = 0$ is suppressed.

In summary, we have investigated quantum charge transport through single C_{60} molecules under the illumination of intense monochromatic THz irradiation. We have achieved the highly efficient focusing of THz waves onto a single-molecule space far beyond the diffraction limit with the aid of metal nanogap electrodes and observed the PAT in SMTs in both the weak coupling and Kondo regimes. The THz power dependence of the PAT conductance indicates that when the incident THz intensity is a few tens of mW, the THz field induced at the molecule exceeds 100 kV/cm, which is enhanced by a factor of 10^5 from the field in the free space. This huge enhancement of the THz field is induced by the plasmonic effect of the nanogap electrode with a bowtie antenna geometry and is on the order of λ/d.

We thank Y. Zhang and S. Q. Du for fruitful discussions and Y. Arakawa for his continuous encouragement. We are also grateful to S. Ishida for his experimental support. This work was partly supported by JST-CREST, Grants-in-Aid from JSPS (No. 25246004 and No. 26706002), MEXT Grant-in-Aid for Scientific Research on Innovative Areas "Science of hybrid quantum systems" (Grant No. 15H05868), Project for Developing Innovation Systems of MEXT, and research grants from the Canon Foundation and the Casio Science Foundation.

*kyoshida@iis.u-tokyo.ac.jp
†Permanent address: Tohoku Institute of Technology, 35-1 Kasumicho, Yagiyama, Taihaku-ku, Sendai, Miyagi 982-8577, Japan.
‡hirakawa@iis.u-tokyo.ac.jp

[1] L. P. Kouwenhoven, N. C. van der Vaart, Y. V. Nazarov, S. Jauhar, D. Dixon, K. McCormick, J. Orenstein,

P. L. McEuen, Y. Nagamune, J. Motohisa, and S. Sakaki, Surf. Sci. **361–362**, 591 (1996).
[2] P. Tien and J. Gordon, Phys. Rev. **129**, 647 (1963).
[3] L. P. Kouwenhoven, S. Jauhar, J. Orenstein, P. L. McEuen, Y. Nagamune, J. Motohisa, and H. Sakaki, Phys. Rev. Lett. **73**, 3443 (1994).
[4] T. H. Oosterkamp, L. P. Kouwenhoven, A. E. A. Koolen, N. C. van der Vaart, and C. J. P. M. Harmans, Phys. Rev. Lett. **78**, 1536 (1997).
[5] Y. Kawano, T. Fuse, S. Toyokawa, T. Uchida, and K. Ishibashi, J. Appl. Phys. **103**, 034307 (2008).
[6] K. Shibata, A. Umeno, K. M. Cha, and K. Hirakawa, Phys. Rev. Lett. **109**, 077401 (2012).
[7] H. Park, J. Park, A. Lim, E. Anderson, A. Alivisatos, and P. McEuen, Nature (London) **407**, 57 (2000).
[8] W. Liang, M. Shores, M. Bockrath, J. Long, and H. Park, Nature (London) **417**, 725 (2002).
[9] J. Park, A. N. Pasupathy, J. I. Goldsmith, C. Chang, Y. Yaish, J. R. Petta, M. Rinkowski, J. P. Sethna, H. D. Aburña, P. L. McEuen, and D. C. Ralph, Nature (London) **417**, 722 (2002).
[10] K. Yoshida, I. Hamada, S. Sakata, A. Umeno, M. Tsukada, and K. Hirakawa, Nano Lett. **13**, 481 (2013).
[11] S. Sakata, K. Yoshida, Y. Kitagawa, K. Ishii, and K. Hirakawa, Phys. Rev. Lett. **111**, 246806 (2013).
[12] P. J. Schuck, D. P. Fromm, A. Sundaramurthy, G. S. Kino, and W. E. Moerner, Phys. Rev. Lett. **94**, 017402 (2005).
[13] D. C. Guhr, D. Rettinger, J. Boneberg, A. Erbe, P. Leiderer, and E. Scheer, Phys. Rev. Lett. **99**, 086801 (2007).
[14] D. R. Ward, N. Grady, C. Levin, N. Halas, Y. Wu, P. Nordlander, and D. Natelson, Nano Lett. **7**, 1396 (2007).
[15] M. A. Seo, H. R. Park, S. M. Koo, D. J. Park, J. H. Knag, O. K. Suwal, S. S. Choi, P. C. M. Planken, G. S. Park, N. K. Park, Q. H. Park, and D. S. Kim, Nat. Photonics **3**, 152 (2009).
[16] D. R. Ward, F. Huser, F. Pauly, J. C. Cuevas, and D. Natelson, Nat. Nanotechnol. **5**, 732 (2010).
[17] H. Park, A. Lim, A. Alivisatos, J. Park, and P. L. McEuen, Appl. Phys. Lett. **75**, 301 (1999).
[18] D. Strachan, D. Smith, D. Johnston, T. Park, M. Therien, D. Bonnell, and A. Johnson, Appl. Phys. Lett. **86**, 043109 (2005).
[19] A. Umeno and K. Hirakawa, Appl. Phys. Lett. **94**, 162103 (2009).
[20] K. Yoshida, A. Umeno, S. Sakata, and K. Hirakawa, Jpn. J. Appl. Phys. **48**, 120216 (2009).
[21] S. Sakata, A. Umeno, K. Yoshida, and K. Hirakawa, Appl. Phys. Express **3**, 115201 (2010).
[22] A. Kogan, S. Amasha, and M. Kastner, Science **304**, 1293 (2004).
[23] J. Elzerman, S. De Franceschi, D. Goldhaber-Gordon, W. van der Wiel, and L. P. Kouwenhoven, J. Low Temp. Phys. **118**, 375 (2000).
[24] B. Hemingway, S. Herbert, M. Melloch, and A. Kogan, Phys. Rev. B **90**, 125151 (2014).
[25] C. Latta, F. Haupt, M. Hanl, A. Weichselbaum, M. Claassen, W. Wuester, P. Fallahi, S. Faelt, L. Glazman, J. von Delft, H. E. Tureci, and A. Imamoglu, Nature (London) **474**, 627 (2011).
[26] M. R. Delbecq, V. Schmitt, F. D. Parmentier, N. Roch, J. J. Viennot, G. Feve, B. Huard, C. Mora, A. Cottet, and T. Kontos, Phys. Rev. Lett. **107**, 256804 (2011).
[27] R. Lopez, R. Aguado, G. Platero, and C. Tejedor, Phys. Rev. Lett. **81**, 4688 (1998).
[28] A. Kaminski, Yu. V. Nazarov, and L. I. Glazman, Phys. Rev. B **62**, 8154 (2000).
[29] P. Nordlander, N. S. Wingreen, Y. Meir, and D. C. Langreth, Phys. Rev. B **61**, 2146 (2000).
[30] L. H. Yu and D. Natelson, Nano Lett. **4**, 79 (2004).
[31] J. J. Parks, A. R. Champagne, G. R. Hutchison, S. Flores-Torres, H. D. Abruna, and D. C. Ralph, Phys. Rev. Lett. **99**, 026601 (2007).
[32] G. D. Scott, Z. K. Keane, J. W. Ciszek, J. M. Tour, and D. Natelson, Phys. Rev. B **79**, 165413 (2009).
[33] D. Goldhaber-Gordon, J. Gores, M. A. Kastner, H. Shtrikman, D. Mahalu, and U. Meirav, Phys. Rev. Lett. **81**, 5225 (1998).
[34] It is known that gold nanoclusters spontaneously formed during the electrical break junction process occasionally serve as Coulomb islands, and exhibit the Kondo effect [A. A. Houck, J. Labaziewicz, E. K. Chan, J. A. Folk, and I. L. Chuang, Nano Lett. **5**, 1685 (2005) H. B. Heersche, Z. de Groot, J. A. Folk, L. P. Kouwenhoven, H. S. J. van der Zant, A. A. Houck, J. Labaziewicz, and I. L. Chuang, Phys. Rev. Lett. **96**, 017205 (2006)]. However, it is reported that in most cases T_K for gold nanoclusters ranges from 5 to 10 K [A. A. Houck, J. Labaziewicz, E. K. Chan, J. A. Folk, and I. L. Chuang, Nano Lett. **5**, 1685 (2005)]. Therefore, the observed T_K (~65 K) strongly suggests that the Coulomb island in the sample is very likely to be a C_{60} molecule. Of course, we cannot completely rule out a possibility that a metal nanocluster of a single-molecule size served as the Coulomb island. However, we would like to emphasize that the physics discussed in this Letter is not affected even in such a case.
[35] The asymmetric tunnel coupling results in a difference in amplitude between the positive, and negative Kondo satellite peaks, and also leads to an asymmetric line shape of the main Kondo resonant peak. Consequently, the satellite peak on the positive-bias side becomes less visible. See also M. Krawiec and K. I. Wysokinski, Phys. Rev. B **66**, 165408 (2002) and F. Simmel, R. H. Blick, J. P. Kotthaus, W. Wegscheider, and M. Bichler, Phys. Rev. Lett. **83**, 804 (1999).
[36] In the peak fitting, we fixed the positions of the satellite conductance peaks at ± 10 mV ($= hf/e$) and assumed that all the peaks have the same width and a symmetric shape.